Chinese Chemical Letters 34 (2023) 108328

Contents lists available at ScienceDirect

Chinese Chemical Letters

journal homepage: www.elsevier.com/locate/cclet

Unraveling the role of phase engineering in tuning photocatalytic hydrogen evolution activity and stability

Jianjian Yi[a,b], Zhou Zhou[a], Yu Xia[a], Ganghua Zhou[a], Guoxiang Zhang[a], Li Li[c], Xuyu Wang[d], Xingwang Zhu[a], Xiaozhi Wang[a,e,f,*], Huan Pang[b,**]

[a] College of Environmental Science and Engineering, Yangzhou University, Yangzhou 225127, China
[b] School of Chemistry and Chemical Engineering, Yangzhou University, Yangzhou 225127, China
[c] Institute for Energy Research, Jiangsu University, Zhenjiang 212013, China
[d] School of Environmental and Chemical Engineering, Jiangsu University of Science and Technology, Zhenjiang 212003, China
[e] Joint International Research Laboratory of Agriculture and Agri-Product Safety of Ministry of Education of China, Yangzhou University, Yangzhou 225127, China
[f] Jiangsu Collaborative Innovation Center for Solid Organic Waste Resource Utilization, Nanjing 210095, China

ARTICLE INFO

Article history:
Received 19 October 2022
Revised 12 February 2023
Accepted 9 March 2023
Available online 13 March 2023

Keywords:
Phase engineering
Hydrogen evolution
Photocatalysis
Cocatalyst
Surface reconstruction

ABSTRACT

In this work, taking $NiSe_2$ as a prototype to be used as cocatalyst in photocatalytic hydrogen evolution, we demonstrate that the crystal phase of $NiSe_2$ plays a vital role in determining the catalytic stability, rather than activity. Theoretical and experimental results indicate that the phase structure shows negligible influence to the charge transport and hydrogen adsorption capacity. When integrating with carbon nitride (CN) photocatalyst forming hybrids (m-$NiSe_2$/CN and p-$NiSe_2$/CN), the hybrids show comparable photocatalytic hydrogen evolution rates (3.26 μmol/h and 3.75 μmol/h). Unlike the comparable catalytic activity, we found that phase-engineered $NiSe_2$ exhibits distinct stability, *i.e.*, m-$NiSe_2$ can evolve H_2 steadily, but p-$NiSe_2$ shows a significant decrease in catalytic process (~57.1% decrease in 25 h). The factor leading to different catalytic stability can be ascribed to the different surface conversion behavior during photocatalytic process, *i.e.*, chemical structure of m-$NiSe_2$ can be well preserved in catalytic process, but partial p-$NiSe_2$ tends to be converted to NiOOH.

Recent studies have demonstrated that, in addition to the composition, size, dimensionality, defect, and facet, crystal phase of nanomaterials plays a crucial role to their catalytic functions [1–3]. Tuning the phase structure of nanomaterials can change the atom arrangement, leading to the regulation of their physical/chemical properties and optimization of catalytic performance [4,5]. With the deepening of relevant understanding, phase engineering is now considered as an effective strategy to optimize materials for efficient catalysis. However, it is still urgent to do research work regarding the following aspects: (1) developing general synthetic methods for the controllable synthesis of desired phases, (2) unmasking the mechanism about the phase transition process, and (3) uncovering the inner mechanism for phase-dependent catalytic activity, stability and selectivity [3,6].

Great efforts have been devoted into material design, controllable synthesis and mechanism exploration, to boost the development of phase engineering toward catalysis. For example, semiconducting 2H-MoS_2 and 2H-$MoSe_2$ have been widely explored as catalysts for hydrogen evolution reaction, but their performances are limited by the poor conductivity and limited active sites at edges [7–9]. Phase engineering strategy can prepare metallic 1T-MoS_2 and 1T-$MoSe_2$, which shows increased charge transfer capacity and active basal plane (chemical insert in 2H phase) [10,11]. As such, improved hydrogen evolution catalysis can be realized. Except for phase transition to metallic 1T phase, phase engineering of MoS_2 from crystalline to amorphous phase can also improve the catalytic hydrogen evolution performance [12]. CO_2 reduction requires more than efficiency, high selectivity to a specific product is of great significance [13]. Phase engineering is also verified that it can affect the selectivity in CO_2 reduction reaction. It was found that, Au nanorods with a well-defined fcc-2H-fcc phase structure show improved CO production selectivity compared to fcc phase Au nanorods in electrocatalytic CO_2 reduction reaction [14]. Deep mechanism study revealed that the reaction energy barrier in the

* Corresponding author at: College of Environmental Science and Engineering, Yangzhou University, Yangzhou 225127, China.
** Corresponding author.
E-mail addresses: xzwang@yzu.edu.cn (X. Wang), panghuan@yzu.edu.cn (H. Pang).

https://doi.org/10.1016/j.cclet.2023.108328
1001-8417/

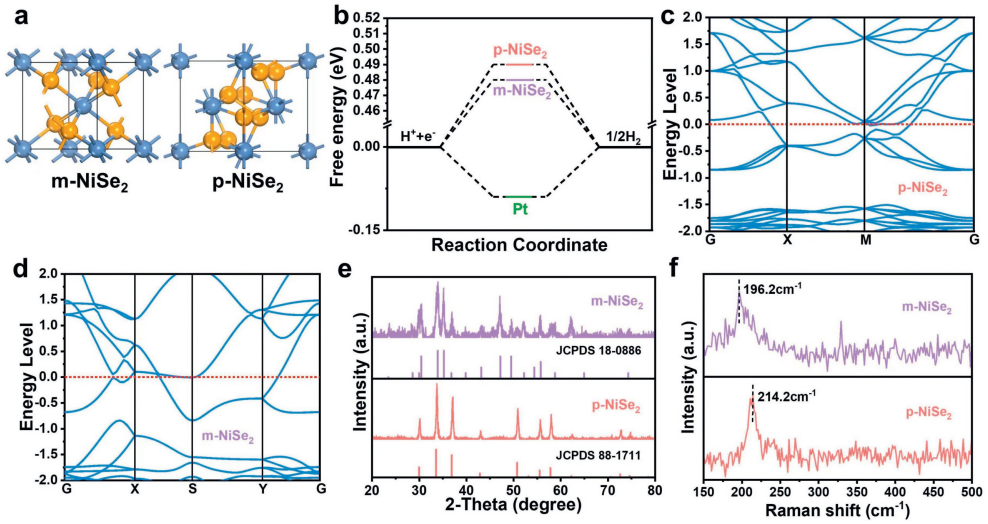

Fig. 1. Theoretical simulation and experimental characterization studies of $NiSe_2$ with different crystal phases. (a) Structure models. (b) The calculated hydrogen adsorption Gibbs free energy (Pt is referred from Ref. [31]). (c, d) The calculated band structures. XRD patterns (e) and Raman spectra (f).

formation of *COOH is decreased at 2H surface and 2H/fcc interface compared to fcc surface, resulting in improved selectivity and activity. Previous case studies have highlighted the fascinating characteristics of phase engineered nanomaterials, and how the catalytic functions are influenced by phase engineering. Despite many phase-engineered nanomaterials have been explored, the understanding of the phase-dependent catalytic performance including activity, selectivity and stability is nowadays still under development.

Photocatalytic hydrogen evolution *via* water splitting is considered as a good research orientation, aiming to mitigating energy and environmental problems in the present century [15–17]. Similar to other typical photocatalytic reactions including CO_2 reduction and N_2 activation, the realization of efficient and stable water splitting is determined by the rational design of catalyst structure, to promote charge separation and molecule adsorption/activation [18,19]. Transitional metal dichalcogenides (TMDs) can serve as cocatalyst on semiconductor surface to boost the photocatalytic hydrogen evolution performance, but their performances are hard to meet the practical requirement regarding both activity and stability, compared to noble metals [6,20,21]. Phase engineering of TMDs offers a feasible avenue to tame the electronic structures and thus improving the catalytic performance. Nickel selenide ($NiSe_2$), a neglected material in TMDs family, has shown potential to catalyze water splitting [22,23]. There are many reported strategies that can tune the property or functions for improved catalysis, for example nanostructure engineering [24], defect engineering [23], constructing heterostructure [22]. However, phase engineering of $NiSe_2$ lacks systematic research. Theoretically, there are two different crystal phases according to the atom arrangement (marcasite phase with orthorhombic structure namely m-$NiSe_2$, and pyrite phase with cubic structure namely p-$NiSe_2$), as presented in Fig. 1a. However, systematic research about the specific role of phase structure for $NiSe_2$ in photocatalytic hydrogen evolution lacks systematic research.

In this communication, we report the phase engineering of $NiSe_2$ and the application in photocatalytic hydrogen evolution, with aims to: (1) develop a general approach for the controllable synthesis of phase-engineered $NiSe_2$, (2) explore the feasibility of improving catalytic activity/stability *via* phase engineering, and (3) uncover the origin of phase-dependent catalytic behaviors. We first developed a simple wet-chemical method to prepare m-$NiSe_2$ and annealing treatment to obtain p-$NiSe_2$, followed by fine characterization of chemical structures. Then, the catalytic hydrogen evolution performance of $NiSe_2$ as cocatalyst was examined by integrating with two-dimensional carbon nitride (2D g-C_3N_4). Finally, we found that the crystal phase structure of $NiSe_2$ plays a vital role in determining the reaction stability, rather than the activity, and discussed the role of phase structure in affecting the activity/stability.

To gain insight into the phase dependent catalytic hydrogen evolution properties of $NiSe_2$, the hydrogen adsorption Gibbs free energy (ΔG_{H^*}), density of state (DOS), and band structure and of $NiSe_2$ based catalysts were theoretically calculated. Fig. 1a and Fig. S1 (Supporting information) illustrate the crystal structures of m-$NiSe_2$ and p-$NiSe_2$, clearly showing the different structures at atomic level. The ΔG_{H^*} of catalyst's surface can provide strong information about the interaction between proton and catalyst's surface. A zero-approaching ΔG_{H^*} with low energy barrier is beneficial for hydrogen evolution reaction [25,26]. In our case, the optimized ΔG_{H^*} values of m-$NiSe_2$ and p-$NiSe_2$ are determined to be 0.48 and 0.49 eV respectively, as shown in Fig. 1b and Fig. S2 (Supporting information). These results indicate that both m-$NiSe_2$ and p-$NiSe_2$ possess appropriate and comparable hydrogen adsorption surfaces, and the hydrogen evolution capacity could not be effectively tuned by phase engineering.

Apart from the ΔG_{H^*}, charge delivery ability is another important parameter affecting the hydrogen evolution performance. As shown in Figs. 1c and d and Fig. S3 (Supporting information), the band structure and DOS of m-$NiSe_2$ and p-$NiSe_2$ were further analyzed. It can be observed that both pure m-$NiSe_2$ and p-$NiSe_2$ show electronic states across the Fermi level, demonstrating their metallic characteristics [27,28]. As such, it can be theoretically predicted that both m-$NiSe_2$ and p-$NiSe_2$ possess good electrochemical conductivity from the theoretical perspective. It can also be noticed that, p-$NiSe_2$ shows only slightly increased numbers of states at Fermi level compared to m-$NiSe_2$, suggesting the comparable intrinsic conductivity theoretically. In summary, theoretical analysis shows that $NiSe_2$ with different crystal phases could both extract the electrons from electrode or light absorber, and possess comparable proton to hydrogen molecule conversion efficiency.

Experimental investigation of the catalytic hydrogen performance for $NiSe_2$ relies on the synthesis of $NiSe_2$ with different crystal phases. The idea of the synthesis is to synthesize metastable state $NiSe_2$ (m-$NiSe_2$) *via* wet chemical method firstly, followed by phase transition to stable state $NiSe_2$ (p-$NiSe_2$) by extra energy input. In this work, we synthesized m-$NiSe_2$ using a

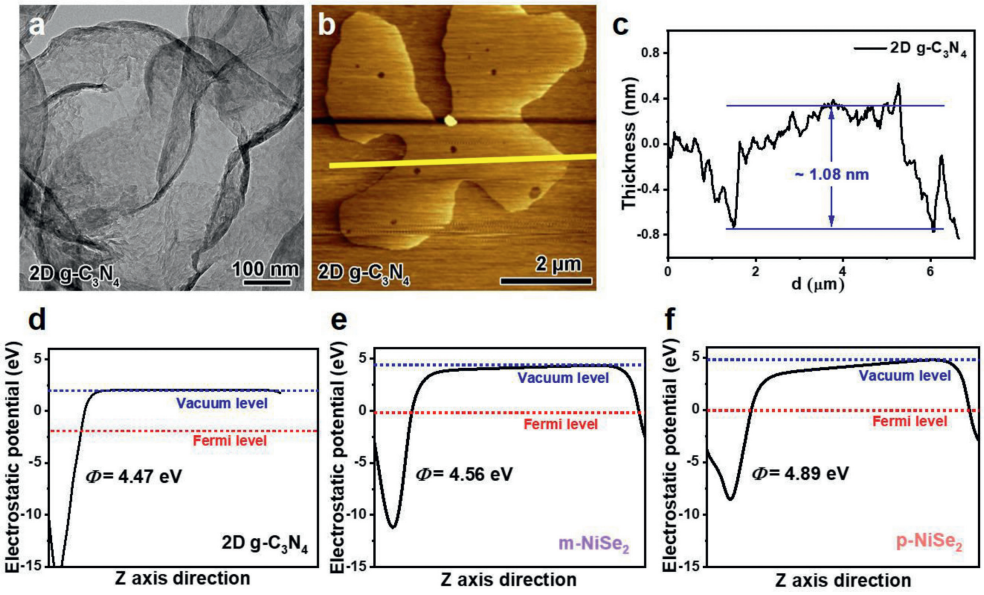

Fig. 2. Structural characterization of 2D g-C_3N_4 and work function simulation. (a) TEM image. AFM image (b) and corresponding height profile (c). (d–f) The calculated work functions of 2D g-C_3N_4, m-$NiSe_2$ and p-$NiSe_2$.

simple wet chemical oil bath method. Phase transition from m-$NiSe_2$ to p-$NiSe_2$ can be realized by a general high-temperature annealing treatment. X-ray diffraction (XRD) was firstly employed to provide structure information of $NiSe_2$ samples, as shown in Fig. 1e. XRD patterns of m-$NiSe_2$ and p-$NiSe_2$ can both be well indexed to the standard PDF cards (JCPDS 18-0886 and JCPDS 88-1711), which preliminarily confirm the successful preparation of phase engineered $NiSe_2$. The phase transition from m-$NiSe_2$ to p-$NiSe_2$ can be further evidenced by Raman analysis. As illustrated in Fig. 1f, two sharp peaks located at 196.2 cm^{-1} and 214.2 cm^{-1} for Se-Se stretching mode were detected. The active peak shift of m-$NiSe_2$ to higher wavelength position for p-$NiSe_2$ is powerful evidence for the changed Se-Se bond length, further illustrating the phase transition from pyrite phase to marcasite phase [29,30]. The surface chemical states and elemental composition were also explored using X-ray photoelectron spectroscopy (XPS) as shown in Fig. S4 (Supporting information), evidencing the fine chemical structure of synthesized $NiSe_2$ samples (detailed illustration in Supporting information).

Upon finely characterizing the chemical structures of $NiSe_2$, the next concern of this work is to investigate the cocatalytic function of phase engineered $NiSe_2$ in photocatalytic hydrogen evolution. In this work, the evaluation of photocatalytic hydrogen evolution performance is based on the selection of carbon nitride nanosheets (2D g-C_3N_4) with stable chemical structure, visible light response and flat surface characteristics, as hosting semiconductor [15,16,32–37]. The large lateral size and specific area are beneficial for the loading of $NiSe_2$, while the ultrathin thickness can effectively shorten the charge migration pathway from bulk to surface, thereby reducing the charge recombination. It can be observed in transmission electron microscopy (TEM, Fig. 2a) image that pristine 2D g-C_3N_4 shows transparent and wrinkled nanosheet morphology. Atomic force microscope (AFM) image and corresponding height profile (Figs. 2b and c) show the lateral size (~5 μm) and thickness corresponding to ~2 atomic layers (~1.08 nm) of 2D g-C_3N_4 [38]. The construction of a typical semiconductor/cocatalyst reaction system is based on the effective charge migration of photogenerated charge carriers from semiconductor to cocatalyst.

Considering that the charge transfer between two components relies on the work function difference, the work functions (Φ) of 2D g-C_3N_4, m-$NiSe_2$ and p-$NiSe_2$ were theoretically calculated to ensure the potential of presented systems (Figs. 2d–f). On the basis that both m-$NiSe_2$ (4.56 eV) and p-$NiSe_2$ (4.89 eV) have larger work function values than pristine 2D g-C_3N_4 (4.47 eV), the charge migration from 2D g-C_3N_4 to $NiSe_2$ after contact can be ensured thermodynamically.

The fabrication process of hybrid photocatalysts is illustrated in Fig. 3a. m-$NiSe_2$ is *in-situ* grown on 2D g-C_3N_4 surface by oil bath reaction using $NiCl_2$ and Se powder as precursors, namely m-$NiSe_2$/CN. As contrast, p-$NiSe_2$/CN can be obtained by a general annealing treatment on m-$NiSe_2$/CN to induce phase transition. XRD patterns and Fourier transform infrared spectra (FT-IR) of the hybrids in Fig. S5 (Supporting information) confirm the coexistence of $NiSe_2$ and 2D g-C_3N_4, and the introduction of $NiSe_2$ does not affect the structure of 2D g-C_3N_4. In the meantime, the morphology and phase structure of as-obtained m-$NiSe_2$/CN and p-$NiSe_2$/CN were analyzed using TEM and high-resolution TEM (HRTEM). TEM images in Fig. S6 (Supporting information) depict that m-$NiSe_2$ and p-$NiSe_2$ with similar nanoribbon morphology are loaded on the surface of sheet-like 2D g-C_3N_4. To disclose the fine phase structure of presented hybrids, HRTEM was performed as shown in Figs. 3b and c. The observed lattice spacings of 0.296 and 0.265 nm in Fig. 3b correspond to (101) and (111) crystal plane of m-$NiSe_2$, while lattice spacings of 0.297 and 0.266 nm in Fig. 3d can be ascribed to (200) and (210) crystal plane of p-$NiSe_2$. The distribution of $NiSe_2$ on 2D g-C_3N_4 surface was also analyzed by scanning TEM (STEM) and corresponding elemental mapping (Figs. 3d and e). The homogeneous distribution of C, N, Ni and Se elements in the catalysts can be observed, clearly showing that $NiSe_2$ with different phases in nanoribbon morphology are anchored uniformly on 2D g-C_3N_4 surface. As contrast, both pristine m-$NiSe_2$ and p-$NiSe_2$ show seriously aggregated morphology as presented in Fig. S7 (Supporting information), suggesting 2D g-C_3N_4 can serve as a good platform for the uniform loading of $NiSe_2$. XPS spectra of m-$NiSe_2$/CN and p-$NiSe_2$/CN were also analyzed as illustrated in Fig. S8 (Supporting information). The Ni 2p spectra and Se 3d spectra are in good agreement with pristine $NiSe_2$ samples, while the C 1s and N 1s spectra are consistent with previous reported g-C_3N_4 [9,15].

Considering the charge migration and highly active surface of $NiSe_2$ with different crystal phases, we are in position to exam-

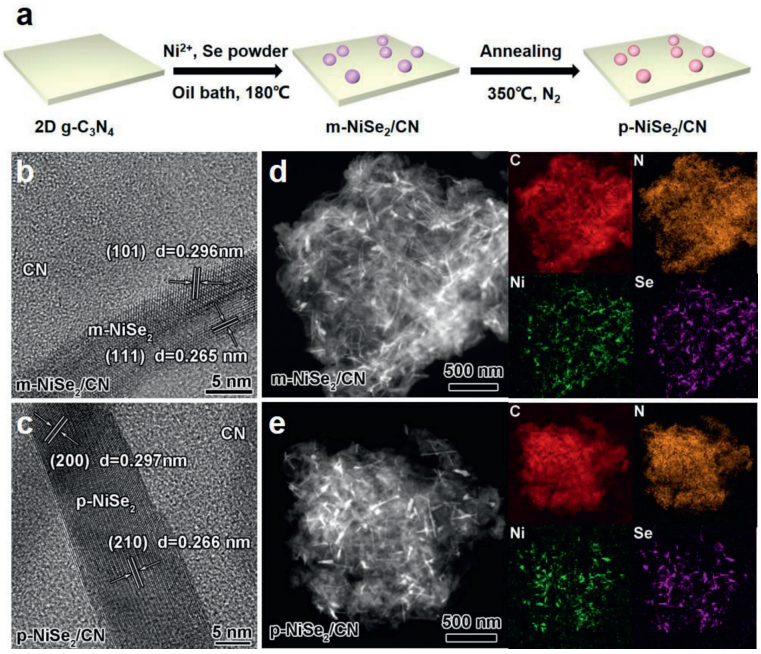

Fig. 3. Structural characterization of m-$NiSe_2$/CN and p-$NiSe_2$/CN. (a) Schematic illustration of construction process. (b, c) HRTEM images. (d, e) STEM and elemental mapping images.

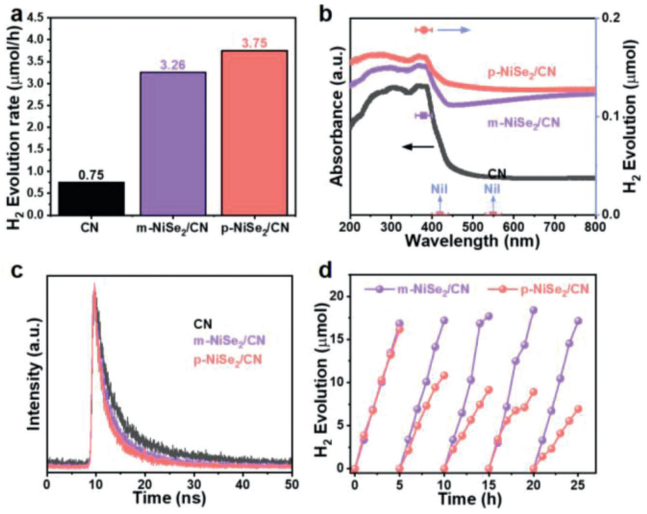

Fig. 4. Hydrogen evolution performance of the catalysts. (a) A comparison of photocatalytic hydrogen evolution rates. (b) Wavelength-dependent hydrogen evolution rates. (c) Transient state fluorescence spectra of the catalysts. (d) Photocatalytic stability evaluation.

ine whether $NiSe_2$ can serve as cocatalyst advancing photocatalytic hydrogen evolution, and investigate the role of crystal phase structures in catalytic hydrogen evolution. The examination of photocatalytic hydrogen evolution performance was then performed using 2D g-C_3N_4 as light absorber, $NiSe_2$ as cocatalysts and TEOA as sacrificial agent under visible light irradiation. As presented in Fig. 4a, it can be firstly found that pristine 2D g-C_3N_4 displays a hydrogen formation rate of 0.75 μmol/h. After merging with $NiSe_2$ cocatalysts, the hydrogen evolution rates can be greatly promoted to 3.26 μmol/h for m-$NiSe_2$/CN and 3.75 μmol/h for p-$NiSe_2$/CN, highlighting the advantages of $NiSe_2$ in promoting charge migration and providing surface active site [20,39]. Despite that many previous reports about phase engineered nanomaterials for hydrogen evolution generally show crystal dependent performance [40–43], in our case, the crystal phase structure of $NiSe_2$ does not play an important role in determining the activity. The reason for this phenomenon is owing to that the phase engineering on $NiSe_2$ leads to negligible optimization on the hydrogen adsorption and charge delivery capacity. Although there is a big gap between $NiSe_2$ and other benchmark cocatalysts (*e.g.*, Pt or MoS_2) for the catalytic performance, the significance and finding for this work can be summarized as below: (i) A universal method is developed for the synthesis of phase-engineered $NiSe_2$; (ii) the effects of phase engineering to catalytic stability is demonstrated over $NiSe_2$; and (iii) the origin for phase-dependent stability is uncovered, which can be owing the different surface reconstruction processes.

To determine the specific role of 2D g-C_3N_4 and $NiSe_2$ in photocatalytic process, the wavelength-dependent hydrogen evolution performance was measured (Fig. 4b). The experimental results illustrate that, H_2 can be evolved when 2D g-C_3N_4 can effectively absorb light irradiation (380 nm monochromatic light) and thus generate charge carriers. Although the introduction of $NiSe_2$ can improve the light absorption in visible light region, not any gas product can be detected under 420 nm and 550 nm monochromatic lights irradiation since $NiSe_2$ with metallic characteristic cannot be excited upon light illumination. The results mentioned above strongly demonstrate the light absorber role of 2D g-C_3N_4 and cocatalyst role of $NiSe_2$.

To uncover the origin of the comparable photocatalytic H_2 evolution activity in $NiSe_2$/CN with different $NiSe_2$ crystal phases, the physicochemical properties of the catalysts were performed to provide insightful information, focusing on light absorption, charge separation and interfacial proton reduction. The light absorption capacity can be evaluated by UV-visible diffuse reflectance spectra (DRS), as can be viewed in Fig. 4b and Fig. S9 (Supporting information). After the introduction of $NiSe_2$, the light absorption in visible light region can be improved due to the black color characteristic of $NiSe_2$. Given the similar light absorption capacity observed in DRS spectra, the charge generation ability based on light harvesting of two $NiSe_2$/CN catalysts are determined to be comparable.

The charge separation efficiency was further determined by transient-state fluorescence (FL), steady state fluorescence spectra

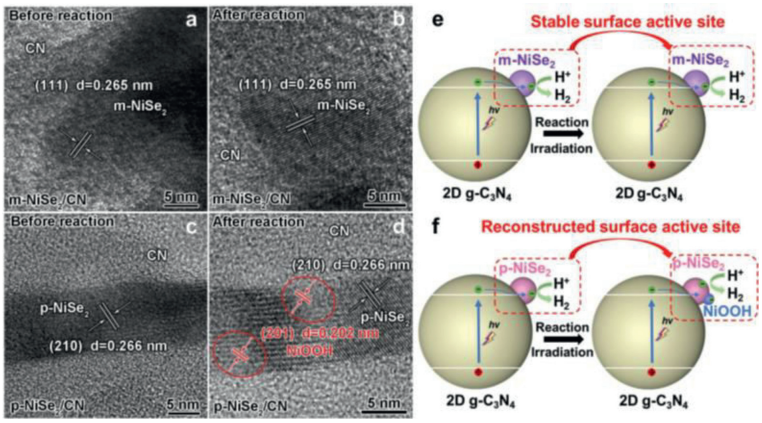

Fig. 5. Morphology and composition analysis of the $NiSe_2$/CN catalysts before and after photocatalytic reaction. (a, b) HRTEM images of m-$NiSe_2$/CN. (c, d) HRTEM images of p-$NiSe_2$/CN catalyst. (e, f) Schematic illustration of the structural transformation of $NiSe_2$ and the effect to photocatalytic processes.

(PL) and photocurrent response. Shorter intensity-average charge lifetimes for m-$NiSe_2$/CN and p-$NiSe_2$/CN compared to pristine CN, can illustrate the enhanced charge separation of 2D g-C_3N_4 after introducing $NiSe_2$ as electron trap (Fig. 4c) [44]. At a meantime, the quenched PL emission (Fig. S10a in Supporting information) and enhanced photocurrent intensity (Fig. S10b in Supporting information) can also support that the loading of $NiSe_2$ can extract photogenerated charge carriers from 2D g-C_3N_4. It should be pointed out that, the charge separation efficiency is also comparable between m-$NiSe_2$/CN and p-$NiSe_2$/CN, based on the characterizations above and theoretical simulations.

The interfacial proton reduction process can be determined by using ΔG_{H^*} as descriptor. As discussed in Fig. 1b, we have demonstrated that both m-$NiSe_2$ and p-$NiSe_2$ can serve as active sites for proton reduction to hydrogen, with calculated of ΔG_{H^*} of 0.48 eV and 0.49 eV respectively. Taken together, it can be concluded that, the introduction of $NiSe_2$ can promote hydrogen evolution since $NiSe_2$ can improve charge separation and provide effective active sites. For photocatalytic hydrogen evolution process, the factors affecting performance includes light absorption, charge separation and surface reactivity. In our case, $NiSe_2$ with different phases can exactly promote the charge separation and provide active site for surface proton reduction, resulting in improved catalysis compared to pristine CN. Since the charge separation efficiency and surface hydrogen adsorption capacity is comparable, the presented m-$NiSe_2$/CN and p-$NiSe_2$/CN exhibited close hydrogen evolution rates.

The stability of m-$NiSe_2$/CN and p-$NiSe_2$/CN was investigated by performing 5 cycles of photocatalytic reaction (25 h). As presented in Fig. 4d, unlike the comparable catalytic activity, it is interesting that m-$NiSe_2$/CN and p-$NiSe_2$/CN show different durability. The hydrogen evolution rate goes steady over m-$NiSe_2$/CN, but almost 50% decrease can be observed in p-$NiSe_2$/CN. Taken the photocatalytic rate measurement result together, it can be demonstrated that, crystal phase engineering on $NiSe_2$ holds the key affecting the catalytic stability, rather than the generally mentioned activity. In general, the most common causes of significant stability changes are the loss or deterioration active components. It has been widely reported that, the surface reconstruction of active sites is a common phenomenon using transitional metal dichalcogenides/nitrides/phosphides as catalysts during catalytic process. For example, it has been demonstrated that the sulfides sometimes can only be considered as pre-catalysts, which will be completely converted to (hydrogen) oxide, or form a sulfide-(hydrogen) oxide core-shell structure [45]. Moreover, it has been found that, metallic Co_4N surface will be transformed to cobalt oxides/hydroxides in electrocatalytic oxygen evolution process [46]. The surface structure reconstruction would thus result in different catalytic activity/stability.

To investigate whether surface structures of $NiSe_2$ were changing with the ongoing of photocatalytic reaction or not, the surface structure transformation behavior of $NiSe_2$/CN catalysts was investigated using HRTEM based on the p-$NiSe_2$/CN and m-$NiSe_2$/CN samples before and after photocatalytic reactions. Fig. S11 (Supporting information) firstly illustrate that the nanosheet structure of 2D g-C_3N_4 can be preserved without significant loss of $NiSe_2$. As can be further viewed from Figs. 5a and b, m-$NiSe_2$ layers on 2D g-C_3N_4 surface could be will preserved after photocatalytic process, without significant observation of other components. As contrast, complete structure of p-$NiSe_2$ is hardly to be seen after reaction, partial lattice spacing corresponding to NiOOH layers can be found around the surface of p-$NiSe_2$ (Figs. 5c and d). The results above reveal that, the formation of NiOOH on p-$NiSe_2$ surface destroyed the pristine active sites, leading to the significant decrease of photocatalytic hydrogen evolution activity. According to the stability test result, it could also be deduced that, the surface reconstruction from p-$NiSe_2$ to NiOOH could reach the steady state after 5 h reaction, since the hydrogen evolution rate becomes relatively stable in 5 h to 25 h (Fig. 4d). To provide more evidence for phase engineering induced stability change, cyclic voltammetry (CV) tests of m-$NiSe_2$ and p-$NiSe_2$ were also performed (Fig. S12 in Supporting information), observing the reduction peak in p-$NiSe_2$ corresponding to Ni^{4+} to Ni^0. As contrast, not any reduction/oxidation peak can be found in m-$NiSe_2$. The CV results can also indirectly support the stable characteristic of m-$NiSe_2$ rather than p-$NiSe_2$ in catalytic process.

Taken together, the role of crystal phase engineering toward photocatalytic hydrogen evolution can be uncovered (Figs. 5e and f). $NiSe_2$ with charge delivery capacity and surface proton reduction ability can serve as an effective cocatalysts for boosting the photocatalytic hydrogen evolution of 2D g-C_3N_4. Upon light illumination, 2D g-C_3N_4 will be excited to generate electron-hole pairs. The photogenerated electrons tend to transfer across the interface to $NiSe_2$ surface, and react with adsorbed protons to evolve H_2 gas product. In our case, phase engineering of $NiSe_2$ exhibits negligible influence to charge transport and hydrogen adsorption capacity, leading to comparable photocatalytic activity between m-$NiSe_2$/CN and p-$NiSe_2$/CN. However, experimental results demonstrate that the crystal phase of $NiSe_2$ plays a vital role in determining the catalytic stability. In photocatalytic process, the surface structure of m-$NiSe_2$ can be preserved, whilst p-$NiSe_2$ surface tends to be transformed to NiOOH, resulting in different stability.

In summary, a facile and effective method is developed to synthesize phase engineered $NiSe_2$ for application in photocatalytic

hydrogen evolution. The hydrogen evolution activity/stability for these different-phased $NiSe_2$ catalysts is also systematically investigated. The results show that m-$NiSe_2$ and p-$NiSe_2$ shows comparable catalytic activity in boosting hydrogen evolution of 2D g-C_3N_4, owing to the similar light harvesting, charge transport and hydrogen adsorption capacity. m-$NiSe_2$ surface is stable during catalytic process while p-$NiSe_2$ tends to be converted to NiOOH, so that m-$NiSe_2$ exhibits better stability than that of p-$NiSe_2$. These results highlight the role of phase engineering in tuning catalytic stability, not limited to activity, and also, suggest that in the process of preparation and screening of catalysts, the materials with high activity/stability can be selected through the regulation of crystalline phase structure.

Declaration of competing interest

The authors declare that they have no known competing financial interests or personal relationships that could have appeared to influence the work reported in this paper.

Acknowledgments

The authors appreciate for the financial support by Natural Science Foundation of Jiangsu Province (No. BK20210827), China Postdoctoral Science Foundation (No. 2021M700117), National Natural Science Foundation of China (Nos. U1904215 and 41977085), Program for Young Changjiang Scholars of the Ministry of Education (No. Q2018270), Six Talent Peaks Project in Jiangsu Province (No. TD-JNHB-012), and 333 Project in Jiangsu Province (No. BRA2020300).

Supplementary materials

Supplementary material associated with this article can be found, in the online version, at doi:10.1016/j.cclet.2023.108328.

References

[1] J. Wu, S. Liu, Y. Rehman, et al., Adv. Funct. Mater. 31 (2021) 2010832.
[2] X. Yin, C.S. Tang, Y. Zheng, et al., Chem. Soc. Rev. 50 (2021) 10087–10115.
[3] Y. Chen, Z. Lai, X. Zhang, et al., Nat. Rev. Chem. 4 (2020) 243–256.
[4] J. Liu, J. Huang, W. Niu, et al., Chem. Rev. 121 (2021) 5830–5888.
[5] H. Li, X. Zhou, W. Zhai, et al., Adv. Energy Mater. 10 (2020) 2002019.
[6] D. Voiry, A. Mohite, M. Chhowalla, Chem. Soc. Rev. 44 (2015) 2702–2712.
[7] Y. Sun, Y. Zang, W. Tian, et al., Energy Environ. Sci. 15 (2022) 1201–1210.
[8] J. Mao, Y. Wang, Z. Zheng, et al., Front. Phys. 13 (2018) 138118.
[9] J. Yi, H. Li, Y. Gong, et al., Appl. Catal. B: Environ. 243 (2019) 330–336.
[10] Y. Yu, G.H. Nam, Q. He, et al., Nat. Chem. 10 (2018) 638–643.
[11] A.R. Puente Santiago, T. He, O. Eraso, et al., J. Am. Chem. Soc. 142 (2020) 17923–17927.
[12] D. Merki, S. Fierro, H. Vrubel, et al., Chem. Sci. 2 (2011) 1262–1267.
[13] J. Fu, K. Jiang, X. Qiu, et al., Mater. Today 32 (2020) 222–243.
[14] Z. Fan, M. Bosman, Z. Huang, et al., Nat. Commun. 11 (2020) 3293.
[15] B. Wu, L. Zhang, B. Jiang, et al., Angew. Chem. Int. Ed. 60 (2021) 4815–4822.
[16] J. Yi, T. Fei, L. Li, et al., Appl. Catal. B: Environ. 281 (2021) 119475.
[17] T. Takata, J. Jiang, Y. Sakata, et al., Nature 581 (2020) 411–414.
[18] B. Wang, W. Zhang, G. Liu, et al., Adv. Funct. Mater. 32 (2022) 2202885.
[19] B. Wang, J. Zhao, H. Chen, et al., Appl. Catal. B: Environ. 293 (2021) 120182.
[20] Q. Zhu, Z. Xu, B. Qiu, et al., Small 17 (2021) e2101070.
[21] T. Rao, H. Wang, Y.J. Zeng, et al., Adv. Sci. 8 (2021) 2002284.
[22] C. Liu, T. Gong, J. Zhang, et al., Appl. Catal. B: Environ. 262 (2020) 118245.
[23] C. Gu, S. Hu, X. Zheng, et al., Angew. Chem. Int. Ed. 57 (2018) 4020–4024.
[24] Z. Huang, S. Yuan, T. Zhang, et al., Appl. Catal. B: Environ. 272 (2020) 118976.
[25] D. Voiry, H.S. Shin, K.P. Loh, et al., Nat. Rev. Chem. 2 (2018) 0105.
[26] J. Ran, G. Gao, F.T. Li, et al., Nat. Commun. 8 (2017) 13907.
[27] Y. Liu, H. Cheng, M. Lyu, et al., J. Am. Chem. Soc. 136 (2014) 15670–15675.
[28] J. Yi, X. Zhu, M. Zhou, et al., Chem. Eng. J. 396 (2020) 125244.
[29] Y.R. Zheng, P. Wu, M.R. Gao, et al., Nat. Commun. 9 (2018) 2533.
[30] X.L. Zhang, S.J. Hu, Y.R. Zheng, et al., Nat. Commun. 10 (2019) 5338.
[31] B. Hinnemann, P.G. Moses, J. Bonde, et al., J. Am. Chem. Soc. 127 (2005) 5308–5309.
[32] I. Krivtsov, D. Mitoraj, C. Adler, et al., Angew. Chem. Int. Ed. 59 (2020) 487–495.
[33] J. Jing, K. Qi, G. Dong, et al., Chin. Chem. Lett. 33 (2022) 4715–4718.
[34] J. Geng, L. Zhao, M. Wang, et al., Environ. Sci.: Nano 9 (2022) 742–750.
[35] K. Qi, J. Jing, G. Dong, et al., Environ. Res. 212 (2022) 113405.
[36] E. Zhao, M. Li, B. Xu, et al., Angew. Chem. Int. Ed. 61 (2022) e202207410.
[37] E. Wang, A. Mahmood, S.-G. Chen, et al., ACS Catal. 12 (2022) 11206–11215.
[38] X. She, J. Wu, J. Zhong, et al., Nano Energy 27 (2016) 138–146.
[39] J. Di, B. Lin, B.J. Tang, et al., Small Struct. 2 (2021) 2100046.
[40] H. Lin, K. Zhang, G. Yang, et al., Appl. Catal. B: Environ. 279 (2020) 119387.
[41] H. Xu, J. Yi, X. She, et al., Appl. Catal. B: Environ. 220 (2018) 379–385.
[42] L. Wang, X. Liu, J. Luo, et al., Angew. Chem. Int. Ed. 56 (2017) 7610–7614.
[43] K. Chang, X. Hai, H. Pang, et al., Adv. Mater. 28 (2016) 10033–10041.
[44] S. Bai, J. Jiang, Q. Zhang, et al., Chem. Soc. Rev. 44 (2015) 2893–2939.
[45] C.X. Zhao, J.N. Liu, C.D. Wang, et al., Energy Environ. Sci. 15 (2022) 3257–3264.
[46] P. Chen, K. Xu, Z. Fang, et al., Angew. Chem. Int. Ed. 54 (2015) 14710–14714.